**Diversified actin protrusions promote environmental exploration but are dispensable for locomotion of leukocytes**

**Authors:** Alexander Leithner[1*], Alexander Eichner[1*], Jan Müller[1,2], Anne Reversat[1], Markus Brown[1,3], Jan Schwarz[1], Jack Merrin[1], David J. J. de Gorter[4], Florian Schur[2], Jonathan Bayerl[2], Ingrid de Vries[1], Stefan Wieser[1], Robert Hauschild[1], Frank P.L. Lai[5], Markus Moser[6], Dontscho Kerjaschki[3], Klemens Rottner[5,7], J. Victor Small[2], Theresia E.B. Stradal[4,5], Michael Sixt[1]

**Affiliations:**

[1] Institute of Science and Technology Austria (IST Austria), am Campus 1, 3400 Klosterneuburg, Austria

[2] Institute for Molecular Biotechnology, Austrian Academy of Sciences, Dr. Bohr-Gasse 3, 1030, Vienna, Austria

[3] Clinical Department of Pathology, Medical University of Vienna, Währinger Gürtel 18-20, 1090 Vienna, Austria

[4]Institute for Molecular Cell Biology, University of Münster, Schlossplatz 5, 48149 Münster, Germany

[5] Helmholtz Centre for Infection Research, Inhoffenstrasse 7, 38124 Braunschweig, Germany

[6] Department of Molecular Medicine, Max Planck Institute of Biochemistry, 82152 Martinsried, Germany

[7] Division of Molecular Cell Biology, Zoological Institute, Technische Universität Braunschweig, Spielmannstrasse 7, 38106 Braunschweig, Germany

*contributed equally

Correspondence: Michael Sixt; Sixt@ist.ac.at, phone +43 2243 90003801

**Key words:**

Cell migration, Actin, Chemotaxis, Leukocyte, Arp2/3, WAVE

**Most migrating cells extrude their front by the force of actin polymerization. Polymerization requires an initial nucleation step, which is mediated by factors establishing parallel filaments in case of filopodia or branch off existing filaments to form the dendritic lamellipodial network. Branches are considered essential for regular cell motility and initiated by the Arp2/3 complex, which in turn is activated by nucleation promoting factors of the WASP and WAVE families[1].**

**Here we employed rapid amoeboid crawling leukocytes and find that deletion of the WAVE complex eliminated actin branching and thus lamellipodia formation. The cells were left with parallel filaments at the leading edge, which translated, depending on the cell type, into a unipolar pointed cell shape or cells with multiple filopodia. Remarkably, unipolar cells migrated with increased speed and enormous directional persistence, while they were unable to turn towards chemotactic gradients. Cells with multiple filopodia retained chemotactic activity but their migration was progressively impaired with increasing geometrical complexity of the extracellular environment. These findings establish that diversified leading edge protrusions serve as explorative structures while they slow down actual locomotion.**

The flat structure of lamellipodia is usually attributed to their surface adhesiveness, and transmembrane coupling of actin dynamics to substrate adhesions is considered to be the basis of the lamellipodium's role in locomotion[1]. Although interference with Arp2/3 activity consistently led to a loss of lamellipodial structures, the reported effects on actual cell motility are variable, with some cells retaining a certain locomotor activity, while others severely slow down or loose their ability to interpret gradients of guidance cues. A common theme of previous studies is, that Arp2/3 controls the organization of adhesive structures and thereby alters motility[2-4]. Notably, most leukocytes are able to migrate in the absence of tight surface adhesions but still form prominent lamellipodia[5]. Hence, the topology of their cytoskeletal organization has a much more immediate impact on cell shape and possibly locomotion, raising the question if and how lamellipodia contribute to low adhesive leukocyte migration. A prototypic example of rapidly migrating leukocytes are dendritic cells (DCs), which earned their name because of their veiled appearance. Especially in their activated state, these cells extend multiple membrane sheets, creating the lettuce-like appearance of a cell with numerous lamellipodia. DCs are highly migratory *in vivo* and in fibrillar 3D environments their locomotion is independent of integrins[6]. DCs exist in two states: immature (iDCs) and mature (mDCs). Maturation is a terminal differentiation step triggered by microbial encounter. It is accompanied by substantial remodeling of the DCs' proteome and initiates rapid migration from peripheral tissues to the draining lymph node, where DCs present peripherally acquired antigen to recirculating T cells[7].

In this study we generate DCs from primary or transiently immortalized precursor cells[8]. Transient immortalization allowed us to introduce stable as well as transient genetic changes. First we dynamically mapped actin, Arp2/3 and nucleation promoting factor localizations in i- and mDCs expressing fluorescent reporters. We focused on WASP and the WAVE complex as the prime candidates to drive Arp2/3 activation at the plasma membrane[9]. Total internal reflection (TIRF) microscopy of i- and mDCs migrating in confined environments revealed dot like actin, Arp2/3, WASP and WAVE patterns in the mid zone of the cell body (Fig. 1A). At the cell front WASP was absent in iDCs but weakly detectable in mDCs (Fig. 1A). In protruding lamellipodia of i- and mDCs, the presence of Arp2/3 was accompanied by the localization of WAVE components in a fine line at the lamellipodial tip. Here WAVE components were enhanced during protrusion and vanished during phases of stagnation or retraction (Fig. 1A and Supplementary movies 1 and 2). Based on these localization data and the absence of significant shape alterations in WASP deficient DCs, we genetically targeted the WAVE complex as the likely driver of lamellipodia formation. To this end, we used conditional gene targeting in mice to delete Hem1 (Supplementary Fig. 1), a subunit of the complex which is specific for the hematopoietic system[10,11]. Hem1-/- DCs showed regular differentiation and none of the three WAVE isoforms was detectable (Supplementary Fig. 2A and B), indicating degradation of the pentameric complex in the absence of Hem1[12,13]. Strikingly, Hem1-/- iDCs lacked the usual lamellipodia and displayed an almost linear needle-like shape, with one sharply pointed front and a rounded rear (Fig. 1B, Supplementary Fig. 2C and Supplementary

movie 3). Similarly, deletion of WAVE2 (another member of the WAVE complex) by CRISPR mediated genome editing in transiently immortalized hematopoietic precursor cells, phenocopied the needle-like shape, excluding WAVE-independent functions as the origin of the phenotype (Supplementary Fig. 2D). In Hem1 deficient cells, no Arp2/3 accumulated at the leading edge, while Arp2/3 and WASP positive dots were still detectable throughout the cell body (Fig. 1C and Supplementary Fig. 2E). Cortical actin appeared unchanged and myosin light chain located to the cell rear as it did in control cells (Supplementary Fig. 2F). Consistent with the loss of lamellipodia, total F-actin levels, as measured by flow cytometric analysis of incorporated phalloidin, were decreased by ~35% (Supplementary Fig. 2G and H). There was no detectable difference in G actin content.

This indicated that cytoskeletal alterations in the mutant cells were restricted to the leading front. While pharmacological disruption of microtubules only mildly altered the shape of Hem1-/- cells, interference with F-actin by latrunculin A as well as treatment with the pan-formin inhibitor SMIFH2[14] led to immediate and complete cell rounding (Fig. 1D). This suggested that the pointed extension is driven by formin-mediated actin-nucleation. To follow up this notion we performed electron tomography to trace actin filaments in situ. Wild type cells showed canonical branch points with a 70° configuration distributed across the lamellipodium[15,16] (Fig. 1E, Supplementary Fig.2I and Supplementary movie 4). In contrast, the pointed edges of Hem1-/- iDCs contained entirely linear arrays of parallel filaments (Fig. 1F and Supplementary Fig.2I) with barbed ends oriented towards the pointed cell edge (Supplementary movie 5)[17]. These findings demonstrate that in the absence of Arp2/3 activation, actin branches at the leading edge are lost and filaments arrange into linear arrays, causing the pointed protrusion morphology.

Notably, upon maturation, Hem1-/- DCs lost their linear shape and the cell bodies rounded up. However, instead of the usual broad and veiled lamellipodial protrusions found in control cells, they formed multiple dynamic, thin filopodial extensions and showed a ~50% reduction in F-actin levels (Fig. 1B, Supplementary Fig. 2C, G and H and Supplementary movie 3). With immature and mature WAVE-complex deficient DCs, we had two morphological cell variants at hand, where lamellipodia were either replaced by one or multiple filopodia. In the following, we utilized these mutants and their respective control counterparts as a tool to dissect the role of lamellipodia and filopodia in guided locomotion within physiological environments.

MDCs use a chemokine receptor, CCR7, to sense the two chemokines, CCL19 and CCL21, which guide the cells from the periphery into the draining lymph node[7]. In order to explore lamellipodial vs. filopodial migration in vivo, we co-injected Hem1-/- and control mDCs into mouse footpads and found that Hem1-/- cells had a competitive disadvantage to reach the draining lymph node (Fig. 2A and B). To determine at which level the cells were impaired we measured migration in mouse ear explants, where chemokine guided interstitial migration vs. entry into the lymphatic vessels can be distinguished. Hem1-/- cells preferentially accumulated at the lymphatic vessel wall, while control cells located in the vessel lumen (Fig. 2B and C). The perivascular accumulation was pronounced even after extended times of

intravasation, indicating that beyond a possible defect in interstitial crawling, the vessel wall represents a rate-limiting barrier for the mutant cells (Supplementary Fig. 3A and B). When we bypassed the peripheral tissue and the vessel wall by directly injecting the cells into afferent lymphatic vessels[18] they equally entered the deep T cell areas (Fig. 2B and D). This shows that the passage through the loose and primarily cellular environment of the lymph node was intact, whereas Hem1-/- mDCs had a possible defect in interstitial crawling and a pronounced defect in intravasation. Intravasation begins with the passage through the endothelial basement membrane, which constitutes a perforated sheet, where cells transiently halt and probe the surface in order to select an appropriate pore for entry[19]. We hypothesized that lamellipodia might act as effective "analogue" exploratory sensors to sample the geometry of the tissue, whereas filopodia have a limited sampling range due to their "digital" configuration. To test sampling in complex environments, we measured chemotaxis through collagen gels of increasing density and, thus, decreasing pore size[20]. In accordance with their shape in suspension, Hem1-/- mDCs migrated with multiple pointed instead of lamellipodial protrusions (Fig. 2E and Supplementary movies 6 and 7). At low collagen concentrations, both control and mutant cells showed efficient chemotaxis (Fig 2F and Supplementary Fig. 3C). However, Hem1-/- mDCs migrated with significantly reduced speed (Fig. 2G). Notably, the disadvantage in speed of Hem1-/- vs. control mDCs increased with the density of the gels and Hem1-/- mDCs were virtually immobilized at high densities where their wild type counterparts still effectively migrated (Fig. 2G and H).

These data are compatible with the idea that lamellipodia are required to make optimal decisions when cells have to thread their cell body and nucleus through geometrically complex environments. However, Arp2/3 might also be involved in the cell body/nuclear passage as such[21]. To dissect these possibilities we devised a series of more reductionist assay systems. We first mimicked barrier and decision-free 1D chemokine driven migration by placing the cells into linear microfluidic channels with a geometry that completely confined the cells (Fig 3A)[22]. Under these conditions, both control and Hem1-/- mDCs migrated efficiently and with no detectable difference in speed (Fig 3B and C). We next introduced constrictions into the channels, which are at the limiting size to allow nuclear passage (Fig 3D)[21]. Rates of passage or passage times were not reduced in Hem1-/- mDCs (Fig 3E and F). After excluding defects in basic locomotion or nuclear passage in Hem1-/- mDCs, we sought to test their ability to make directional choices. To this end, we established microfluidic devices that confined the cells in the z dimension while the x y-field was built of road-blocks positioned with variable spacing. This essentially creates a maze that cells have to negotiate in order to follow chemokine gradients (Fig 3G). Control, as well as Hem1-/- cells, efficiently navigated along the gradients, but now Hem1-/- mDCs were considerably slower than control cells (Fig 3H and Supplementary movie 8). To measure protrusion dynamics, we determined the average change of cell area per frame. This was significantly reduced for Hem1-/- cells compared to their wild type counterparts while overall cell size was unaffected (Fig 3I and Supplementary Fig. 3D). This suggests that, when confronted with multiple directional

choices, their reduced protrusion dynamics gives Hem1-/- mDCs a competitive disadvantage over control cells in efficiently negotiating complex environments.

We next compared the migration of unipolar Hem1-/- iDCs with control iDCs. When placed in low-density 3D collagen scaffolds, control cells showed vivid protrusion dynamics, but net displacements were minimal due to frequent directional changes (Fig. 4A and B, Supplementary movie 9). Strikingly, Hem1-/- cells migrated with substantially increased speed (Fig. 4C) and showed massively increased directional persistence (Fig. 4A, Supplementary Fig. 4A). During migratory phases the cells maintained their linear shape (Fig. 4B and Supplementary movie 10) and the rare directional changes were either associated with transient arrest and rounding or with occasional bifurcation of the leading edge (Supplementary movie 10). Bifurcations consistently caused deceleration (Supplementary Fig. 4B and Supplementary movie 10). Importantly, also control cells showed phases of straight and fast migration and these were associated with elongated morphology. This was shown quantitatively by a correlation between shape index and migratory speed (Supplementary Fig. 4C). These observations support the idea that diversification of the leading edge effectively slows locomotion[23,24]. This might potentially explain the gain in migration speed of unipolar Hem1-/- iDCs compared to their control counterparts.

To test the chemotactic response of WAVE complex-deficient iDCs, we incorporated them into 3D collagen gels and exposed them to gradients of CCL3. In contrast to wild type controls, Hem1-/- as well as WAVE2-/- iDCs showed only minimal responses to chemotactic gradients (Fig. 4D and E and Supplementary Fig. 4D and E). Notably, the chemokinetic response of both mutants and controls followed the same dynamics, suggesting that chemokine sensing, signaling or signal adaptation was unimpaired (Fig 4F). In line with these data, signaling upon chemokine exposure was unimpaired (Fig. 4G and Supplementary Fig. 4F) when measured biochemically at the level of phosphorylation of downstream targets.

These data suggest that lamellipodia and filopodia primarily serve as directional selectors in these cells[25,26], while the main forces driving actual locomotion might be generated elsewhere. To directly probe the role of lamellipodia in force transduction, we devised a microfluidic setup where leukocytes migrate confined between two parallel surfaces[27] (Fig. 5A). This reductionist setting allowed cells to efficiently migrate under minimal adhesive conditions in an actin dependent manner[5]. When migrating DCs expressing an actin reporter were simultaneously imaged with widefield and TIRF microscopy, it turned out that lamellipodial actin rarely contacted the substrate, while the cell body formed a continuous interface, where retrograde actin flow was minimal compared to the lamellipodial region (Fig. 5B and Supplementary movie 11). We obtained comparable data with migrating lymphoblasts and neutrophil granulocytes (Fig 5C and D and Supplementary movie 11) but not with adhesively migrating fish keratocytes, which form large lamellipodia in continuous contact with the substrate (5E and Supplementary movie 11). Fast confocal observation of migrating mDCs expressing Abi1-GFP, which decorates the lamellipodial tip, confirmed that

lamellipodia are neither in contact with bottom nor top-surfaces, thereby largely undulating in the free space between the confining surfaces (Fig 5F and G and Supplementary movie 12).

Together, we show that in fast migrating leukocytes, actin driven protrusions in the form of lamellipodia and filopodia facilitate directional choices and invasion of complex matrices, while actual translocation is driven by the cell body[28] (Supplementary Figure 5). This mechanism differs from mesenchymal migration[29], where adhesions are born in the lamellipodium and thereby determine cell shape and mediate translocation. Migration with a freely exploring lamellipodium is more in line with bleb-driven locomotion where the (actin free) cell front is unlikely to participate in force transduction and friction with the substrate mainly emerges in the central regions of the cell[30,31]. We therefore suggest that the leukocytes lamellipodium is rather a sensory organelle than a force-transducing unit.

**References**


1. Skau, C. T. & Waterman, C. M. Specification of Architecture and Function of Actin Structures by Actin Nucleation Factors. *Annu. Rev. Biophys.* **44,** 285–310 (2015).
2. Rotty, J. D., Wu, C. & Bear, J. E. New insights into the regulation and cellular functions of the ARP2/3 complex. *Nat Rev Mol Cell Biol* (2012). doi:10.1038/nrm3492
3. Wu, C. *et al.* Arp2/3 Is Critical for Lamellipodia and Response to Extracellular Matrix Cues but Is Dispensable for Chemotaxis. *Cell* **148,** 973–987 (2012).
4. Suraneni, P. *et al.* The Arp2/3 complex is required for lamellipodia extension and directional fibroblast cell migration. *The Journal of Cell Biology* **197,** 239–251 (2012).
5. Renkawitz, J. *et al.* Adaptive force transmission in amoeboid cell migration. *Nature Publishing Group* 1–19 (2009). doi:10.1038/ncb1992
6. LAmmermann, T. *et al.* Rapid leukocyte migration by integrin-independent flowing and squeezing. *Nature* **453,** 51–55 (2008).
7. Heuzé, M. L. *et al.* Migration of dendritic cells: physical principles, molecular mechanisms, and functional implications. *Immunol. Rev.* **256,** 240–254 (2013).
8. Redecke, V. *et al.* hematopoietic progenitor cell lines with myeloid and lymphoid potential. *Nature Methods* 1–13 (2013). doi:10.1038/nmeth.2510
9. Campellone, K. G. & Welch, M. D. A nucleator arms race: cellular control of actin assembly. *Nat Rev Mol Cell Biol* **11,** 237–251 (2010).
10. Hromas, R., Collins, S., Raskind, W., Deaven, L. & Kaushansky, K. Hem-1, a potential membrane protein, with expression restricted to blood cells. *Biochim. Biophys. Acta* **1090,** 241–244 (1991).
11. Weiner, O. D. *et al.* Hem-1 Complexes Are Essential for Rac Activation, Actin Polymerization, and Myosin Regulation during Neutrophil Chemotaxis. *PLoS Biol* **4,** e38 (2006).
12. Blagg, S. L., Stewart, M., Sambles, C. & Insall, R. H. PIR121 Regulates Pseudopod Dynamics and SCAR Activity in Dictyostelium. *Current Biology* **13,** 1480–1487 (2003).
13. Kunda, P., Craig, G., Dominguez, V. & Baum, B. Abi, Sra1, and Kette Control the Stability and Localization of SCAR/WAVE to Regulate the Formation of Actin-Based Protrusions. *Current Biology* **13,** 1867–1875 (2003).
14. Rizvi, S. A. *et al.* Identification and Characterization of a Small Molecule Inhibitor of Formin-Mediated Actin Assembly. *Chemistry & Biology* **16,** 1158–1168 (2009).
15. Svitkina, T. M. & Borisy, G. G. Arp2/3 complex and actin depolymerizing factor/cofilin in dendritic organization and treadmilling of actin filament array in lamellipodia. *The Journal of Cell Biology* **145,** 1009–1026 (1999).
16. Vinzenz, M. *et al.* Actin branching in the initiation and maintenance of lamellipodia. *Journal of Cell Science* **125,** 2775–2785 (2012).
17. Narita, A. *et al.* Direct Determination of Actin Polarity in the Cell. *Journal of Molecular Biology* **419,** 359–368 (2012).
18. Braun, A. *et al.* Afferent lymph–derived T cells and DCs use different chemokine receptor CCR7–dependent routes for entry into the lymph node and intranodal migration. *Nat Immunol* **12,** 879–887 (2011).
19. Pflicke, H. & Sixt, M. Preformed portals facilitate dendritic cell entry into afferent lymphatic vessels. *Journal of Experimental Medicine* **206,** 2925–2935 (2009).
20. Wolf, K. *et al.* Physical limits of cell migration: control by ECM space and nuclear deformation and tuning by proteolysis and traction force. *The Journal of Cell Biology* **201,** 1069–1084 (2013).
21. Thiam, H.-R. *et al.* Perinuclear Arp2/3-driven actin polymerization enables nuclear deformation to facilitate cell migration through complex environments. *Nature Communications* **7,** 1–14 (2016).
22. Heuzé, M. L., Collin, O., Terriac, E., Lennon-Dumenil, A.-M. & Piel, M. in *Methods in Molecular Biology* **769,** 415–434 (Humana Press, 2011).
23. Pankov, R. A Rac switch regulates random versus directionally persistent cell migration. *The Journal of Cell Biology* **170,** 793–802 (2005).
24. Dang, I. *et al.* Inhibitory signalling to the Arp2/3 complex steers cell migration. *Nature* 1–19 (2013). doi:10.1038/nature12611
25. Insall, R. H. Understanding eukaryotic chemotaxis: a pseudopod-centred view. 1–6 (2010). doi:10.1038/nrm2905
26. Arrieumerlou, C. & Meyer, T. A Local Coupling Model and Compass Parameter for Eukaryotic Chemotaxis. *Developmental Cell* **8,** 215–227 (2005).

27. Le Berre, M., Zlotek-Zlotkiewicz, E., Bonazzi, D., Lautenschlaeger, F. & Piel, M. *Methods forTwo-DimensionalCell Confinement. Methods in Cell Biology - Volume 97* **121,** 213–229 (Elsevier Inc., 2014).
28. Stanley, P. *et al.* Intermediate-affinity LFA-1 binds α-actinin-1 to control migration at the leading edge of the T cell. *EMBO J* **27,** 62–75 (2007).
29. Case, L. B. & Waterman, C. M. Integration of actin dynamics and cell adhesion by a three-dimensional, mechanosensitive molecular clutch. *Nat. Cell Biol.* **17,** 955–963 (2015).
30. Kardash, E. *et al.* A role for Rho GTPases and cell–cell adhesion in single-cell motility in vivo. *Nat. Cell Biol.* **12,** 47–53 (2009).
31. Bergert, M. *et al.* Force transmission during adhesion-independent migration. *Nat. Cell Biol.* **17,** 524–529 (2015).
32. Riedl, J. *et al.* Lifeact: a versatile marker to visualize F-actin. *Nature Methods* **5,** 605–607 (2008).
33. Lai, F. P. L. *et al.* Arp2/3 complex interactions and actin network turnover in lamellipodia. *EMBO J* **27,** 982–992 (2008).
34. Benesch, S. *et al.* Phosphatidylinositol 4,5-biphosphate (PIP2)-induced vesicle movement depends on N-WASP and involves Nck, WIP, and Grb2. *J. Biol. Chem.* **277,** 37771–37776 (2002).
35. Steffen, A. *et al.* Sra-1 and Nap1 link Rac to actin assembly driving lamellipodia formation. *EMBO J* **23,** 749–759 (2004).
36. Behrndt, M. *et al.* Forces Driving Epithelial Spreading in Zebrafish Gastrulation. *Science* **338,** 257–260 (2012).
37. Small, J. V., Herzog, M. & Anderson, K. Actin filament organization in the fish keratocyte lamellipodium. *The Journal of Cell Biology* **129,** 1275–1286 (1995).
38. Winkler, C., Vinzenz, M., Small, J. V. & Schmeiser, C. Actin filament tracking in electron tomograms of negatively stained lamellipodia using the localized radon transform. *J. Struct. Biol.* **178,** 19–28 (2012).
39. To appear in Nature Protocol Exchange
40. Maiuri, P. *et al.* Actin Flows Mediate a Universal Coupling between Cell Speed and Cell Persistence. *Cell* **161,** 374–386 (2015).

**Acknowledgements:**

This work was supported by the German Research Foundation (DFG) Priority Program SP 1464 to T.S and M.S, and European Research Council (ERC GA 281556) and Human Frontiers Program grants to M.S. We thank Hans Haecker for his generous help with HoxB8 immortalization, Jörg Renkawitz for critical reading of the manuscript and the Scientific Service Units of IST Austria for excellent technical support.

**Competing financial interests:**

The authors declare that they have no competing financial interests.

**Figure 1. Localization of Arp2/3 activation machinery and morphologies of wt and hem1-/- DCs.** (**A**) Snapshots of TIRF microcopy of i- and mDCs expressing reporter constructs for ArpC5, WASP and Abi1. Insets show kymographs and histograms of fluorescence intensity along yellow lines in main figures. Scale bar, 10µm. (**B**) SEM pictures of wt and hem1-/- i- and mDCs. All scale bars, 5µm. (**C**) Snapshots of TIRF microscopy of hem1-/- iDCs expressing reporter constructs for ArpC5 and WASP. Scale bar, 10µm. (**D**) Quantification of hem1-/- iDC cell shape in suspension upon pharmacological treatment, dotted line denotes separate experiments. Mean ± S.D., *left:* one-way ANOVA, *right:* two-tailed t-test, **** P<0.0001. n=8 samples per treatment from 2 (left) or 3 (right) biologically independent experiments. (**E**) *Left*: Electron tomography of wt iDC. Scale bar, 5µm. *Right*: section of the lamellipodium marked by yellow square in left picture. Scale bar, 100nm. Inset: detail of branch junction marked by yellow square. (**F**) *Left*: Electron tomography of hem1-/- iDC. Scale bar, 5µm. *Middle*: section of the tip marked by yellow square in left picture. Scale bar, 100nm. *Right*: detail of parallel actin filaments marked by yellow square in middle picture. Scale bar, 20nm.

**Figure 2. Migratory properties of wt and hem1-/- mDCs *in vivo* and *in vitro*. (A)** Ratio of differentially labeled wt/wt and hem1-/-/wt mDCs in LNs of wt recipient mice, 24h after footpad injection. Mean (red line) ± S.D. (black bars). Two-tailed t-test, **** P<0.0001. n=10 LNs (wt/wt), n=19 LNs (hem1-/-/wt) from one (wt/wt) or two (hem1-/-/wt) biologically independent experiments. (**B**) Scheme of experiments shown in A, C and D. D=dermis, DC=dendritic cell, E=epidermis, LN=lymph node, LV=lymph vessel. (**C**) *Left:* Ratios of wt and hem1-/- mDCs inside/outside of LVs 2h after application to ears. Blue and green dots, connected with a line represent data from one ear. Two-tailed t-test, ** P=0.0034. n=12 ears from 2 biologically independent experiments. *Right:* Z-projection of intravasation assay 2h after application of wt (green) and hem1-/- (magenta) mDCs. LVs are stained with Lyve-1 (white). Inset: detail of region marked by white square. Scale bar, 100µm. (**D**) *Left*: Average distance (µm) of differentially labeled wt and hem1-/- mDCs from LN capsule, 4.5h after intralymphatic injection. Blue and green dots, connected with a line represent data from one LN. Two-tailed t-test (log transformed), not significant P=0.6. n=11 LNs from one biological replicate. *Right*: Example of LN 4.5h after intralymphatic co-injection of wt (red) and hem1-/- (green) mDCs. LN is stained for smooth muscle actin (SMA, blue). Scale bar, 300µm. (**E**) Time lapse sequence of migrating wt and hem1-/- mDCs in response to CCL19 in 3D collagen gels. Cells are pseudo colored in green. Scale bars, 20µm. (**F**) Tracks of wt and hem1-/- mDCs in response to CCL19 gradient in 3D collagen gels. (**G**) Single cell speeds (µm/min.) of wt and hem1-/- mDCs in response to CCL19 gradient, depending on increasing rattail collagen concentrations. Mean (red line) ± SEM (black bars). Two-tailed t-tests (sqrt transformed for 1.7 mg/ml), **** P<0.0001. n=82/80/81 cells (wt: 1.1/1.7/2.3 mg/ml), n=80/81/80 cells (hem1-/- : 1.1/1.7/2.3 mg/ml) from 3 biologically independent experiments. (**H**) Ratio of average displacement per frame of hem1-/- / wt mDCs towards CCL19 source, depending on

increasing rattail collagen concentrations. Mean (green dots) ± SEM (black bars). Data stem from the same 3 biological replicates as in (**G**).

**Figure 3. Migratory properties of wt and hem1-/- mDCs in microfluidic devices.** (**A**) Scheme of experimental setup for (**B**) and (**C**). (**B**) Time lapse sequence and exemplary kymographs of wt and hem1-/- mDCs migrating towards CCL19 source in straight microchannels. (**C**) Single cell speeds (µm/min.) of wt and hem1-/- mDCs in response to CCL19 gradient, migrating in straight microchannels. Mean (red line) ± SD (black bars). Two-tailed t-test, n.s. P=0.0773. n=82 cells (wt), n=83 cells (hem1-/-) from 2 biologically independent experiments. (**D**) Scheme of experimental setup for (**E**) and (**F**). (**E**) Percentage of wt and hem1-/- mDCs passing constriction when migrating towards CCL19 gradient in absence (dark colors) or presence (light colors) of 50µM Blebbistatin. SD (black bars). Fishers exact test, wt (n=118 cells) vs. hem1-/- (n=73 cells): n.s. P=1, wt 50µM Blebbi (n=56 cells) vs. hem1-/- 50 µM Blebbi (n=89 cells): n.s. P=0.1439. untreated vs. 50 µM Blebbi: **** P<0.0001. 3 biological replicates. (**F**) Single cell passage times through constriction of wt and hem1-/- mDCs migrating towards CCL19 gradient. Mean (red line) ± SD (black bars). Two-tailed t-test (log transformed), n.s. P=0.0586. n=74 cells (wt), n=62 cells (hem1-/-) from 3 biological replicates. (**G**) Scheme of 'maze' setup for (**H**) and (**I**). (**H**) Speeds (µm/min.) of single cell tracks from wt and hem1-/- mDCs in response to CCL19 gradient, migrating in microfluidic 'maze' device. Mean (red line) ± SD (black bars). Mann-Whitney test, **** P<0.0001. n=214 tracks (wt), n=180 tracks (hem1-/-) from 3 biologically independent experiments. (**I**) Mean change in cell area per frame in percent, relative to previous frame of single wt and hem1-/- mDCs migrating in microfluidic 'maze' device. Mean (red line) ± SD (black bars). Mann-Whitney test, *** P=0.0004. n=20 cells (wt), n=21 cells (hem1-/-). Data stem from the same 3 biological replicates as in (**H**).

**Figure 4. Migratory properties of wt and hem1-/- iDCs.** (**A**) Single cell tracks of wt and hem1-/- iDCs migrating in 3D collagen gels. (**B**) Time laps sequence of migrating wt and hem1-/- iDCs migrating in 3D collagen gels. Scale bars, 20µm. (**C**) Single cell speeds (µm/min.) of wt and hem1-/- iDCs migrating in 3D collagen gel. Mean (red line) ± S.D. (black bars). Two-tailed t-test (sqrt transformed), **** P<0.0001. n=120 cells (wt), n=120 cells (hem1-/-) from 3 biologically independent experiments. (**D**) Single cell tracks of wt and hem1-/- iDCs in response to CCL3 gradient in 3D collagen gels. (**E**) Average y-displacement (pixel/min.) over time (min.) of wt (blue) and hem1-/- (green) iDCs in absence (triangles) or response (circles) to CCL3 gradient. Mean (dots and triangles) ± SEM (black bars). 3 biologically independent experiments. (**F**) Average fold increase in speed over time (min.) of wt and hem1-/- iDCs in response to CCL3 gradient compared to no chemokine. Mean (Green and blue lines). Data stem from the same 3 biological replicates as in (**E**). (**G**) Western blots against phosphorylated Akt and GAPDH of wt and hem1-/- iDCs stimulated with CCL3 chemokine.

**Figure 5. Lamellipodial position of leukocytes during confined migration.** (**A**) Scheme depicting experiments in panels B–D. (**B-E**) Brightfield and TIRF (red) time-lapse sequence of wt mDC, T cell, neutrophil (migrating under confinement) and fish keratocyte. Yellow dotted lines outline the rim of the lamellipodium. White lines mark kymographs plotted on the right. All scale bars, 5µm. (**F**) Oblique top- and front view false color time-lapse z-reconstructions of wt mDC expressing Abi1-eGFP. Scale bar oblique top view: 10µm. Scale bar front views: 3µm. White lines in front views mark kymograph plotted in (**G**).

**Figure 1.**

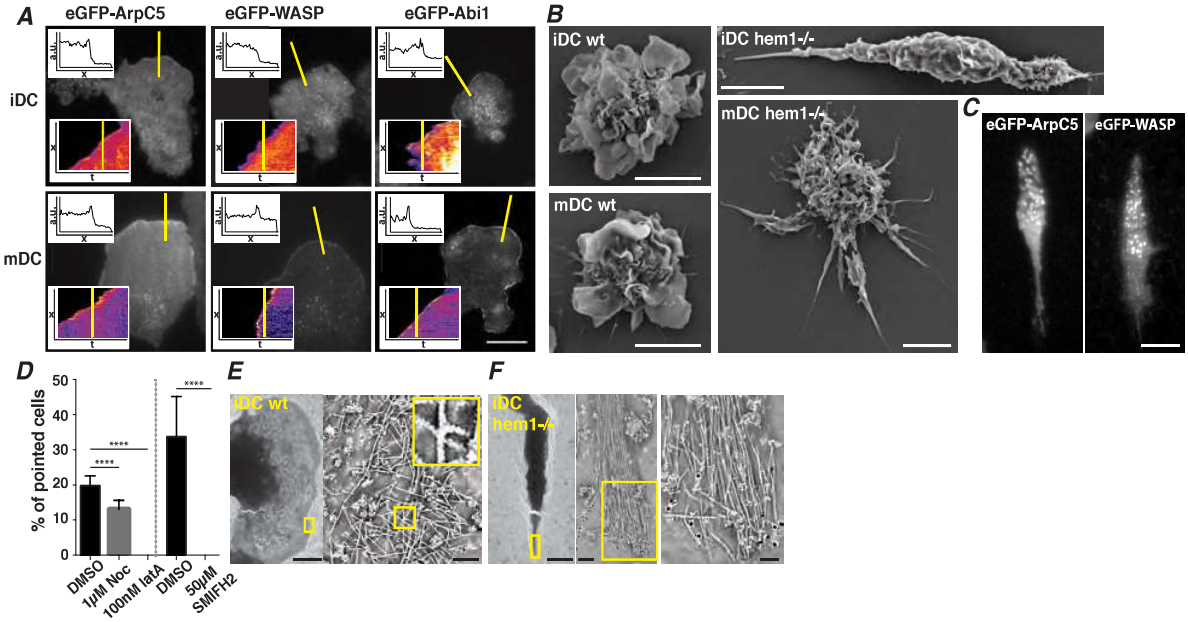
A
eGFP-ArpC5
eGFP-WASP
eGFP-Abi1
iDC
mDC
B
iDC wt
iDC hem1-/-
mDC wt
mDC hem1-/-
C
eGFP-ArpC5
eGFP-WASP
D
% of pointed cells
50
40
30
20
10
0
****
****
****
DMSO
1µM Noc
100nM latA
DMSO
50µM SMIFH2
E
iDC wt
F
iDC hem1-/-

**Figure 2.**

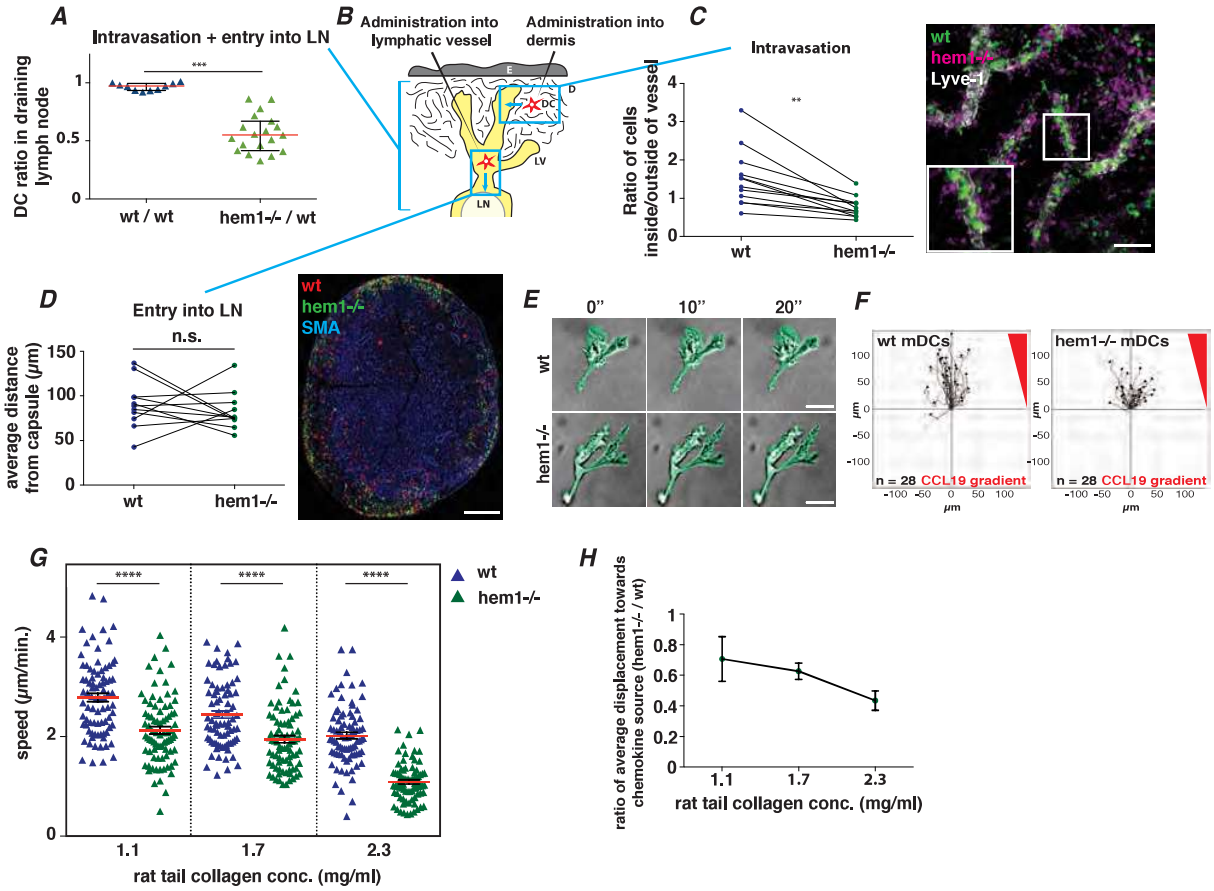
A
Intravasation + entry into LN
DC ratio in draining lymph node
wt / wt
hem1-/- / wt
B
Administration into lymphatic vessel
Administration into dermis
E
D
DC
LV
LN
C
Intravasation
Ratio of cells inside/outside of vessel
wt
hem1-/-
wt
hem1-/-
Lyve-1
D
Entry into LN
n.s.
average distance from capsule (μm)
wt
hem1-/-
SMA
E
0"
10"
20"
F
wt mDCs
hem1-/- mDCs
n = 28 CCL19 gradient
μm
G
speed (μm/min.)
wt
hem1-/-
rat tail collagen conc. (mg/ml)
H
ratio of average displacement towards chemokine source (hem1-/- / wt)
rat tail collagen conc. (mg/ml)

**Figure 3.**

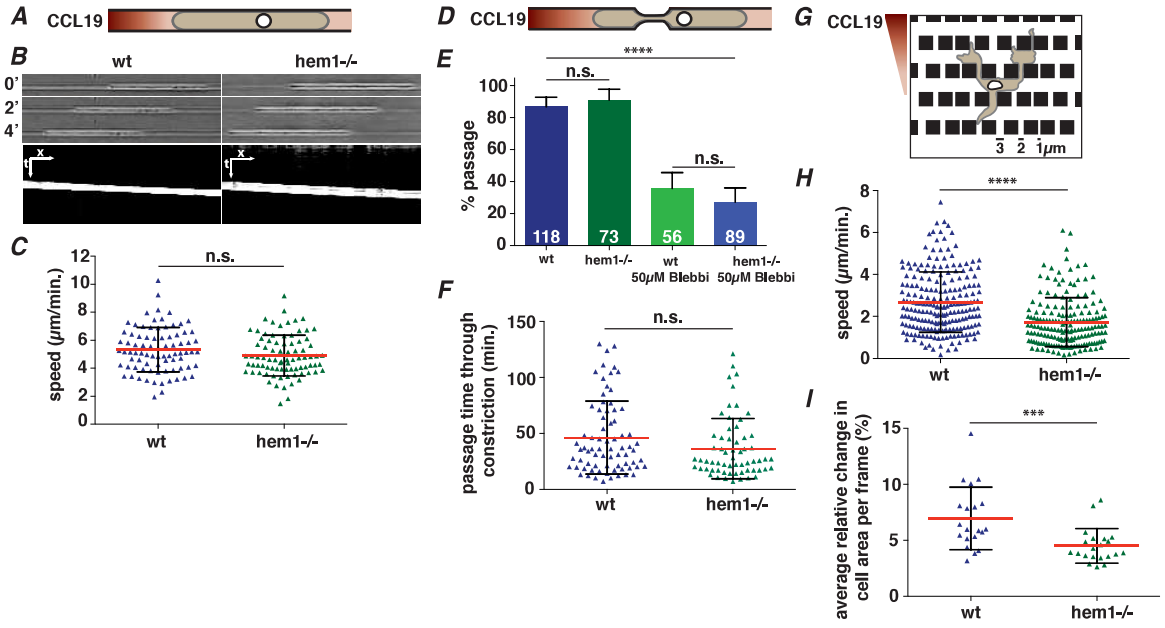
A
CCL19
B
wt
hem1-/-
0'
2'
4'
C
speed (μm/min.)
n.s.
wt
hem1-/-
D
CCL19
E
% passage
****
n.s.
n.s.
118
73
56
89
wt
hem1-/-
wt
50μM Blebbi
hem1-/-
50μM Blebbi
F
passage time through constriction (min.)
n.s.
wt
hem1-/-
G
CCL19
3
2
1μm
H
speed (μm/min.)
****
wt
hem1-/-
I
average relative change in cell area per frame (%)
***
wt
hem1-/-

**Figure 4.**

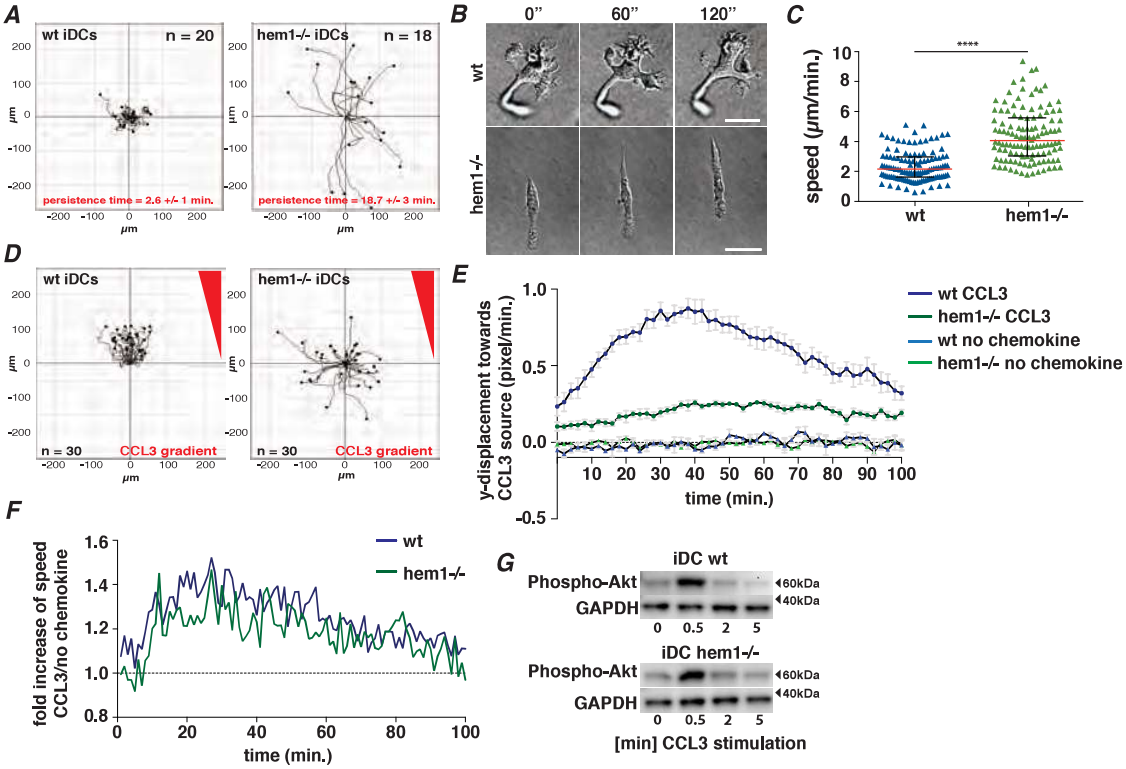
A
wt iDCs
n = 20
persistence time = 2.6 +/- 1 min.
hem1-/- iDCs
n = 18
persistence time = 18.7 +/- 3 min.
μm
B
0"
60"
120"
wt
hem1-/-
C
****
speed (μm/min.)
wt
hem1-/-
D
wt iDCs
n = 30
CCL3 gradient
hem1-/- iDCs
n = 30
CCL3 gradient
E
wt CCL3
hem1-/- CCL3
wt no chemokine
hem1-/- no chemokine
y-displacement towards CCL3 source (pixel/min.)
time (min.)
F
wt
hem1-/-
fold increase of speed CCL3/no chemokine
time (min.)
G
iDC wt
Phospho-Akt
GAPDH
60kDa
40kDa
0 0.5 2 5
iDC hem1-/-
Phospho-Akt
GAPDH
60kDa
40kDa
0 0.5 2 5
[min] CCL3 stimulation

**Figure 5.**

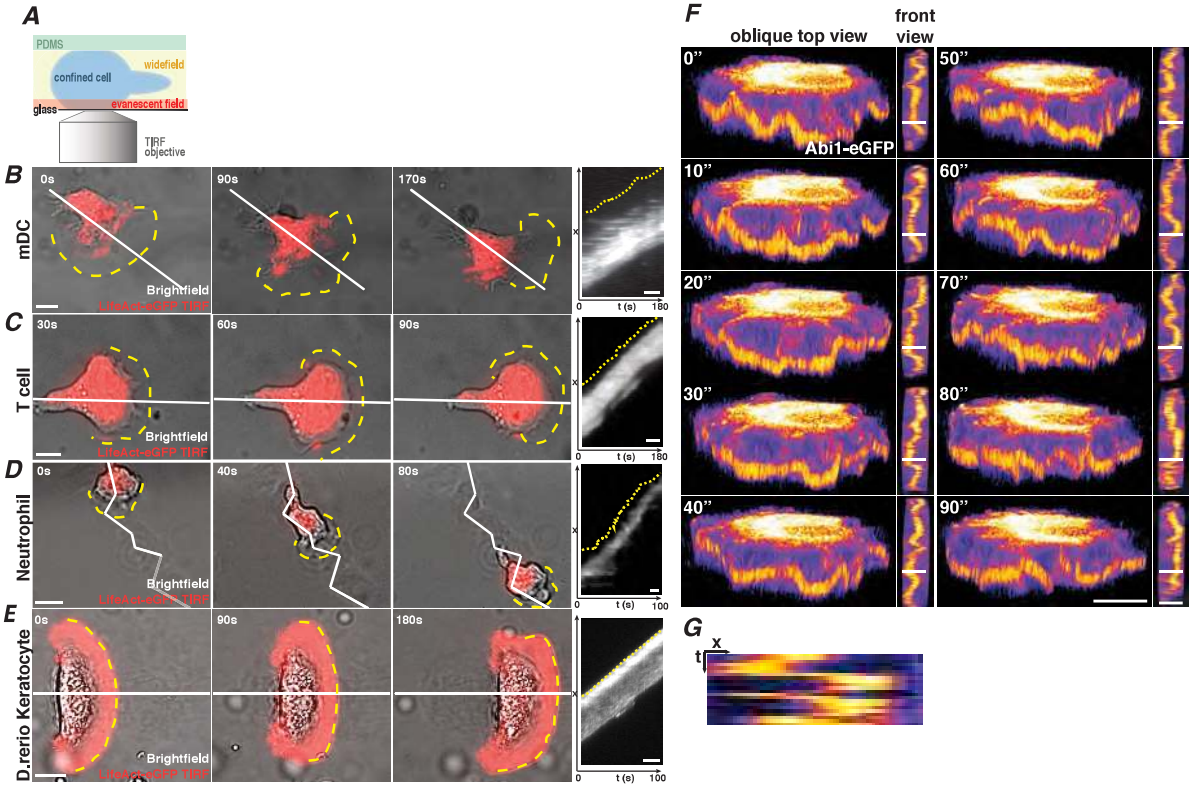
A
PDMS
confined cell
widefield
glass
evanescent field
TIRF objective
B
mDC
0s
90s
170s
Brightfield
LifeAct-eGFP TIRF
C
T cell
30s
60s
90s
D
Neutrophil
0s
40s
80s
E
D.rerio Keratocyte
0s
90s
180s
t (s)
F
oblique top view
front view
Abi1-eGFP
0”
10”
20”
30”
40”
50”
60”
70”
80”
90”
G
x
t

**Supplementary Figure 1.**

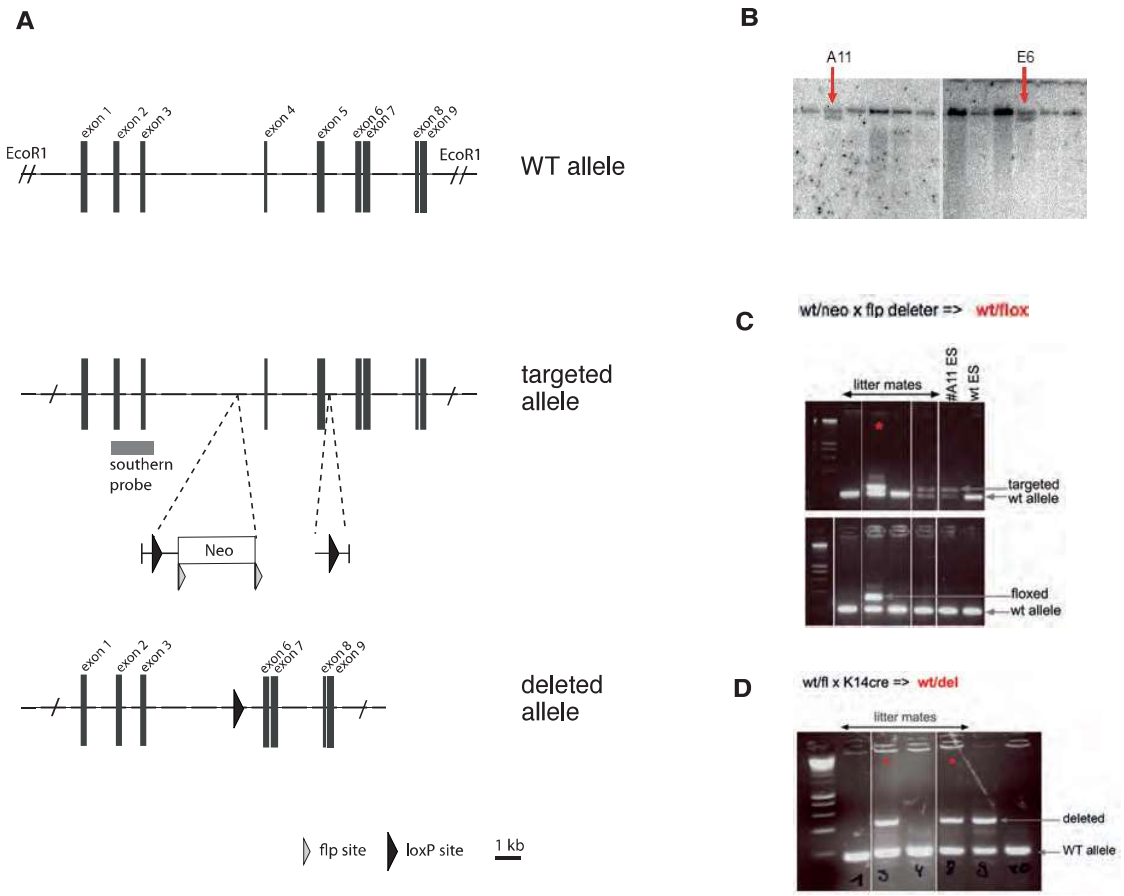

# Supplementary Figure 2.

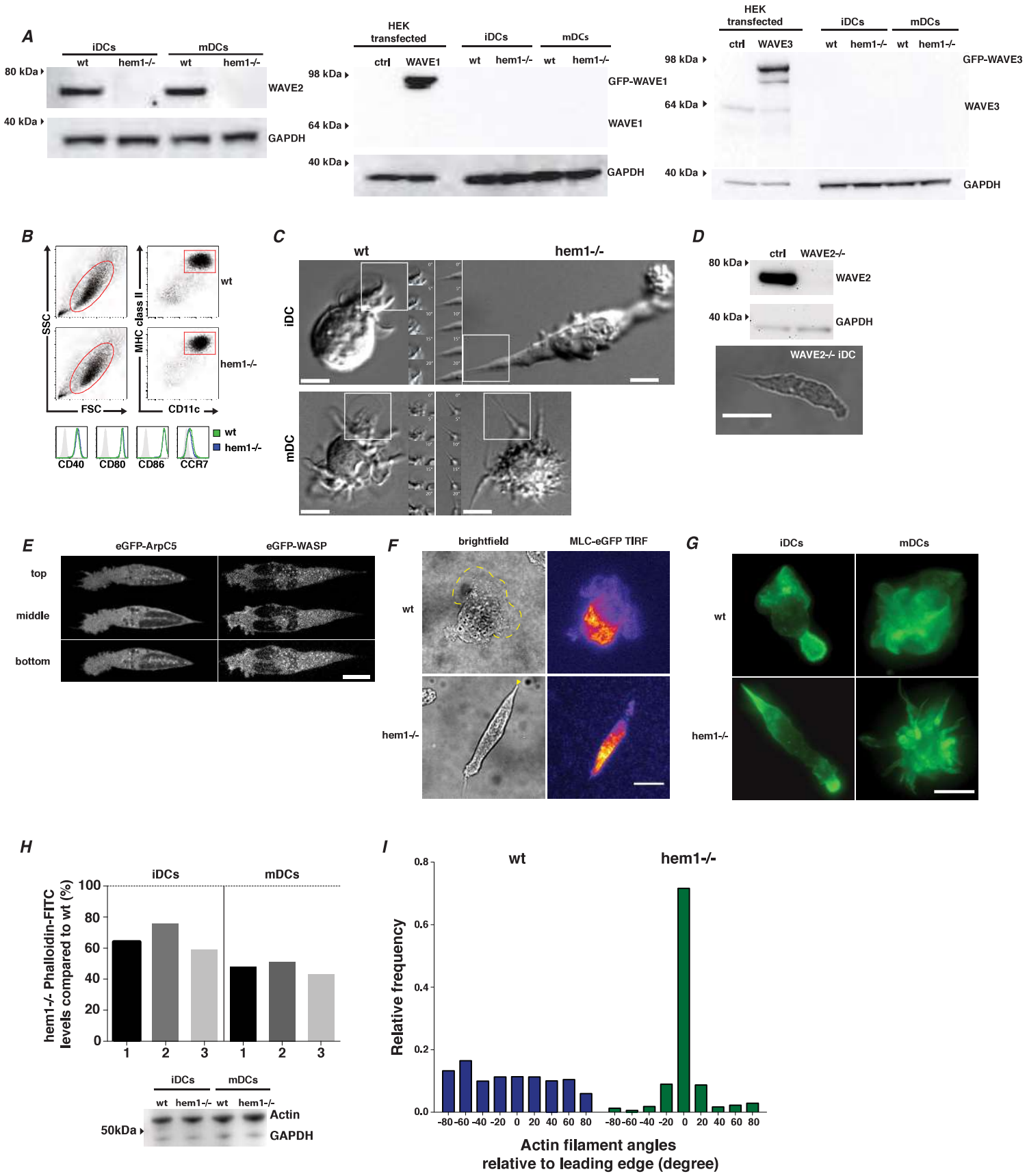

## Supplementary Figure 3.

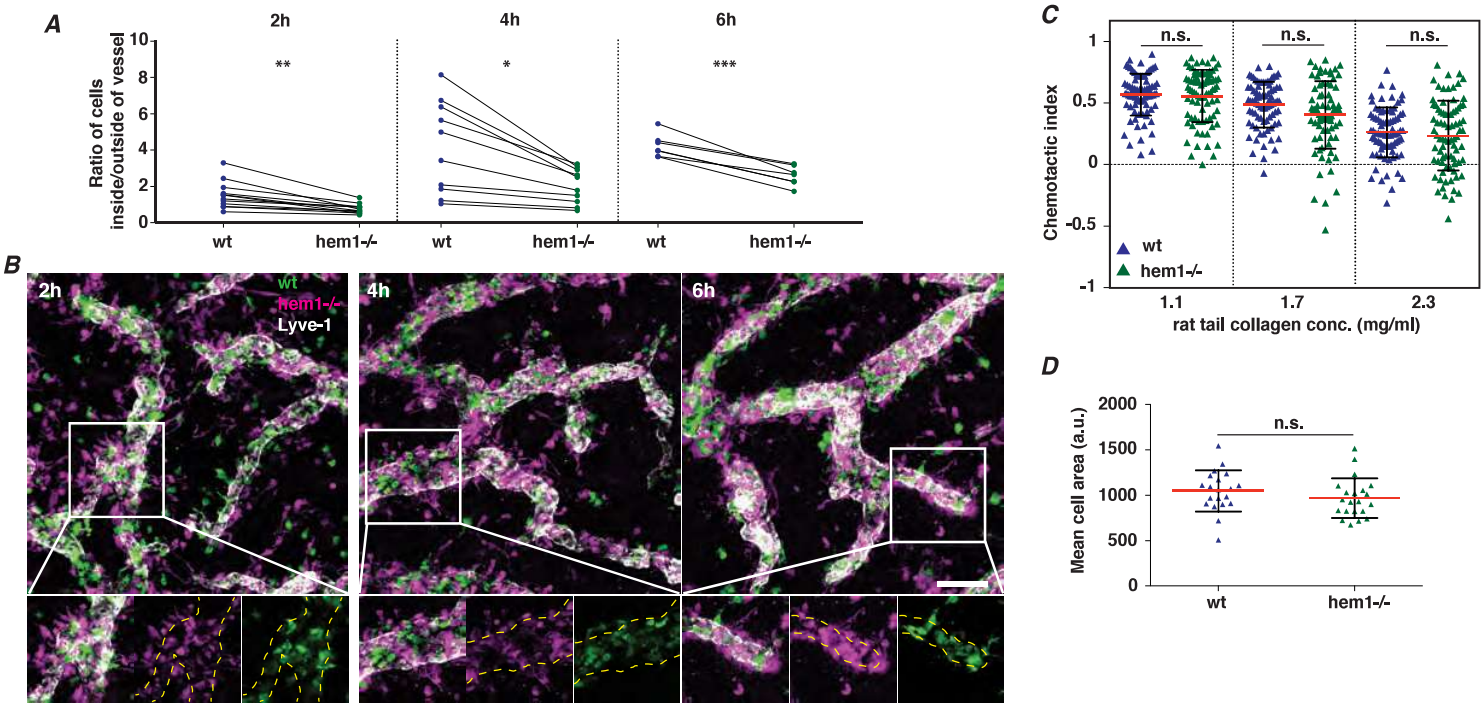

## Supplementary Figure 4.

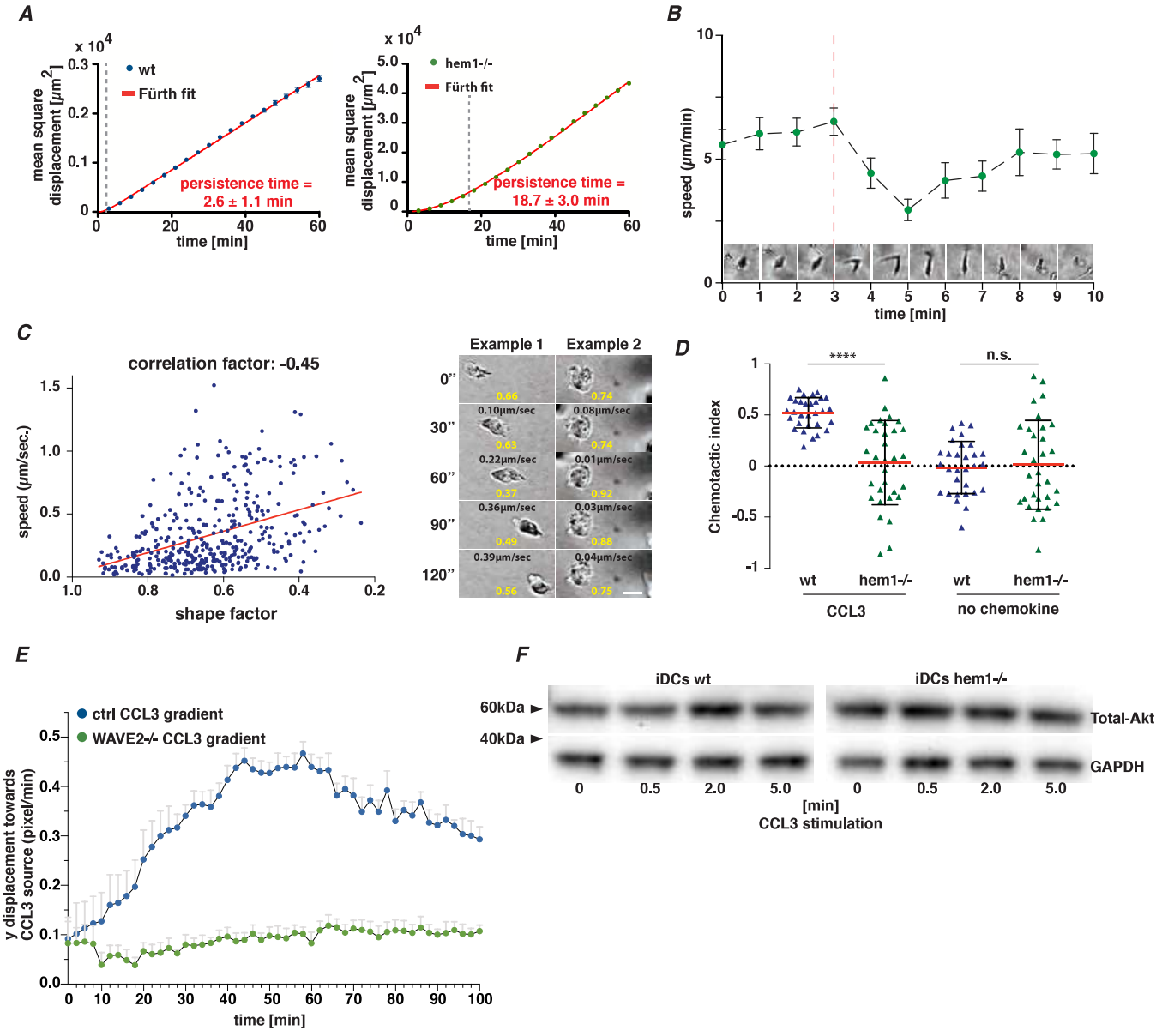

**Supplementary Figure 5.**

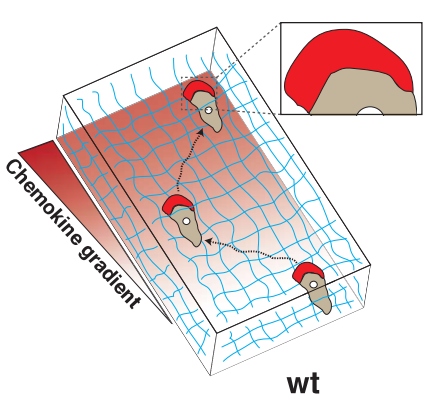


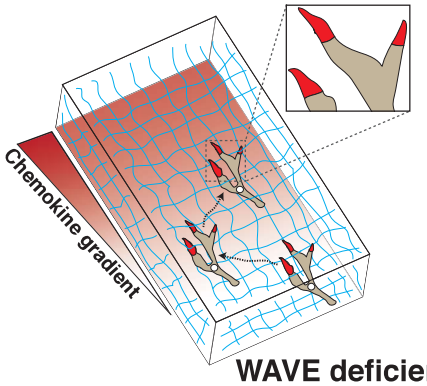


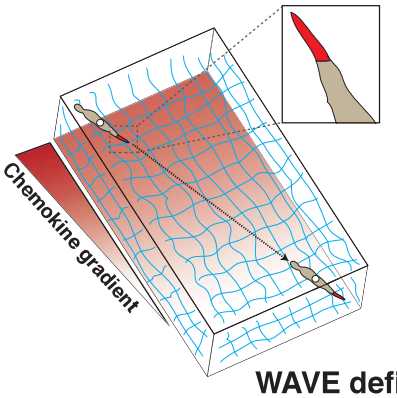


| | wt i-/mDCs | WAVE deficient mDCs | WAVE deficient iDCs |
|---|---|---|---|
| **Locomotion** | + | + | ++ |
| **Gradient sensing** | + | + | + |
| **Navigation** | ++ | + | - |

**Supplementary Figure 6.**